Terr. Atmos. Ocean. Sci., Vol. 19, No. 3, 309-319, June 2008 doi: 10.3319/TAO.2008.19.3.309(AA)

# A Study of Precipitation Effect on Tropospheric Electromagnetic Wave Propagation at Frequency 19.5 GHz

Shun-Peng Shih[1, *]

[1] *Department of Computer and Communication, Shu-Te University, Kaohsiung, Taiwan 824, ROC*

Received 11 May 2006, accepted 7 August 2007

**ABSTRACT**

In this article, we take advantage of a terrestrial propagation link at Ka-band 19.5 GHz located on the campus of the National Central University in Chung-Li City to carry out a tropospheric radio propagation experiment. Data collected in 2004 were used in data analysis to provide a deeper understanding of the precipitation effect on tropospheric electromagnetic wave propagation at Ka-band. The results indicate that the relation between specific attenuation $\kappa_e$ of 19.5 GHz radio wave amplitude and the measured rain fall rate R (in unit of mm $hr^{-1}$) is of the form: $\kappa_e = aR^b$ (in unit dB $km^{-1}$) with a = 0.0699 and b = 1.0984, which is fairly close to that obtained by assuming Laws-Parsons drop size distribution. In order to study the overall attenuation characteristics of Ka-band radio wave influenced by precipitation particles, we used a ground-based 2D disdrometer to measure the terminal velocities of raindrops and their size distributions. The result shows that the relation between raindrop diameter and terminal velocity in terms of the Power-Law relation, i.e., $V(D) = AD^B$, and the drop size distribution can be expressed in the form of a Gamma distribution function, i.e., $N(D) = N_0D^{\mu}\exp(-\delta D)$. With these results, the corresponding rain attenuation of the electromagnetic wave at Ka-band is estimated and discussed in this article.

Key words: Precipitation, Rain attenuation, Ka-band, Drop size distribution, Terrestrial propagation link

*Citation: Shih, S. P., 2008: A study of precipitation effect on tropospheric electromagnetic wave propagation at frequency 19.5 GHz. Terr. Atmos. Ocean. Sci., 19, 309-319, doi: 10.3319/TAO.2008.19.3.309(AA)*

## 1. INTRODUCTION

Recent years have seen rapid development in wireless communication technology worldwide. The development of technologies in satellite communications, digital image transmissions, multimedia applications, Internet and mobile communications etc. have led to increased demand for data transmission capacity and placed massive pressure on present-day radio bands, which have become over crowded and difficult to grow due to their relatively low frequencies. Consequently, emphasis in data transmission technology has switched to high-frequency microwave bands. The main reasons being their relatively wide frequency bandwidth and relatively large channel capacity make them suitable for receiving large volumes of data with little influence from the ionosphere. Therefore use of microwaves at Ka-band for the purposes of satellite and terrestrial communications represents an irreversible future trend (Shih and Chu 1999).

Link propagation reliability is a key issue concerning the design of satellite and terrestrial communication systems. Propagation effects may impair the availability and quality of satellite and terrestrial communication systems during service periods, particularly at higher frequencies, such as those of the Ka-band. Therefore, extensive knowledge of propagation phenomena affecting system availability and signal quality in this band is required (Hasanuddin et al. 2002).

Generally speaking, the propagation of electromagnetic waves within the Ka-band is readily susceptible to precipitation particles (Crane 1996). As a result, they can seriously impair the quality of surface-to-satellite or surface-to-surface communications (Bussey 1950; Crane 1971; Hogg and Chu 1975), leading to rain attenuation of wave energy. It is well known that the physical processes involved in the cause of the rain attenuation are absorption and the scattering by precipitation particles. In addition, depolarization effect caused by the non-spherical shape of raindrops can also exert an influence on the attenuation of signals within

* *Corresponding author*
*E-mail: spshih@mail.stu.edu.tw*

the Ka-band. Besides which, scintillation of signals, which is caused by diffraction resulting from the irregularity of the atmospheric refraction index and refraction generated by electromagnetic waves having to pass through such a highly stratified atmospheric structure, plays a very important role in the communication link for ground and satellite systems. Hence, when we use the Ka-band as the frequency for surface-to-surface or surface-to-satellite communications, the propagation channels for these communications will be affected by atmospheric precipitation, resulting in the attenuation of signal intensity.

Precipitation particles in the atmosphere are can be either liquid in form, solid or melting. Of these particles, solids have very little effect on the attenuation of electromagnetic waves, so in general they can be neglected in quantitatively estimating rain attenuation of the propagation channel at the Ka-band (Battan 1973). However, in the region of the zero-degree centigrade isothermal layer, a liquid water membrane covers solid precipitation particles due to melting. Compared to solid precipitation particles, the refraction indexes of liquid rain drops are larger than those of solids, causing backscatter from the former of about 6.74 dB greater than that of the latter. When electromagnetic waves of the Ka-band propagate in the rain, their wavelengths are equivalent to the particle diameters of raindrops, i.e., generally less than 0.5 cm. The scattering of electromagnetic waves of the Ka-band is in accordance with the Mie Scattering theory, rather than that of Rayleigh scattering. On the basis of measurements from a ground-based disdrometer located on the campus of the National Central University, we will quantitatively estimate the magnitude of rain attenuation in the Ka-band for the case of Mie scattering in this article.

In general, the relation between rain attenuation (Ar) and the surface rain fall rate in terms of their effect on terrestrial or surface-to-satellite communication links can be expressed in the form: $Ar = L(Rp)\kappa_e(Rp)$, where $\kappa_e(Rp)$ is the specific attenuation of precipitation in unit of dB $km^{-1}$; Rp is the rain fall rate in unit of mm $hr^{-1}$; and L(Rp) is the effective path length of electromagnetic waves in the precipitation area (Rice and Holmberg 1971; Ippolito 1986). The relation between $\kappa_e(Rp)$ and Rp can be obtained theoretically and/or experimentally, and generally is expressed as $\kappa_e(Rp) = aR^b$ (Olsen et al. 1978), in which a and b are the functions of the frequency of radio waves, drop size distribution, and rain temperature. Some investigators have verified the power law relation between specific attenuation and the rain fall rate in terms of measured data; the empirical values of a and b were also estimated accordingly (Harrold 1967; Samplak and Turrin 1969). Therefore, we can conclude that the higher the precipitation is, the stronger the attenuation of electromagnetic waves will be. Normally, when the frequency of electromagnetic waves is more than 10 GHz, the precipitation particle will be the main cause for the attenuation of communication signals (Oguchi 1983).

Although theoretical and experimental studies of rain attenuation can be found in many papers (Crane 1980; Dissanayake et al. 1997; Karasawa and Maekawa 1997; Polonio and Riva 1998), measured rain attenuation data is still insufficient for estimating the link within an individual spot beam. In this article, we will take advantage of an experimental Ka-band propagation system at 19.5 GHz located on the campus of the National Central University in Chungli City to carry out a terrestrial rain attenuation experiment. The purpose of this experiment is to understand to what extent attenuation of EM waves of the Ka-band is affected by surface rain fall in northern Taiwan. Expressly, a study of the characteristics of the Ka-band propagation channel in the presence of precipitation can help establish a rain attenuation model in the Taiwan region for the use of surface-to-satellite and/or terrestrial communication links at the Ka-band.

## 2. THEORETICAL CONSIDERATIONS

When Ka-band electromagnetic waves are propagating in a precipitation environment, the physical processes responsible for the attenuation of the incident waves are the absorption and scattering of the precipitation particles distributed along the wave propagation path. It is worth noting that most rain drops are between 0.5 mm - 0.5 cm in diameter, which is approximately the wavelength of electromagnetic waves in the Ka-band. Therefore, in order to quantitatively analyze the precipitation effect on the characteristics of Ka-band EM wave propagation, Mie theory need first be applied to establish a theoretical model for estimating corresponding rain attenuation.

The effect of precipitation particles on the amplitude (or power) attenuation of electromagnetic waves with in the Ka-band is related to the effective path length of EM wave propagation, wave frequency, drop size distribution, and rain temperature etc. Therefore, prior to establishing a quantitative relation to estimate the magnitude of rain attenuation of electromagnetic waves with in the Ka-band caused by precipitation particles, the theoretical extinction coefficients, namely the scattering and absorbing coefficients based on the Mie theory must first be calculated. We define the parameters $\chi$ and n below (Ulaby et al. 1981):

$$\chi = \kappa_b \cdot r = \frac{2\pi r}{\lambda_b} = \frac{2\pi r}{\lambda_0}\sqrt{\varepsilon'_{rb}} \tag{1}$$

and

$$n = \frac{n_p}{n_b} = \left(\frac{\varepsilon_{cp}}{\varepsilon_{cb}}\right)^{1/2} \equiv \varepsilon_c^{1/2} \tag{2}$$

where r is the radius of the raindrop; $\kappa_b$ is the wave number of the electromagnetic waves in the background medium; $\varepsilon'_{rb}$ is the real part of the relative dielectric constant of the background medium; $\lambda_b$ is the wavelength of the electromagnetic waves in the background medium; $\lambda_0$ is the wavelength of the electromagnetic waves in free space; $n_p$ and $n_b$ represent the complex refraction indexes of precipitation particles and background medium, respectively while $\varepsilon_{cp}$ and $\varepsilon_{cb}$ represent the relative complex dielectric constants. When the background medium is the atmosphere, we have $\varepsilon'_{rb} = 1$, $n_b = 1$, and $\lambda_b = \lambda_0$.

To proceed, the relation between fall velocity with respect to still air and raindrop size should be adopted for the development of the theoretical model of rain attenuation. In this work, two models of fall (or terminal) velocity V versus raindrop diameter D are used. Namely, one is the Atlas model and the other one is the power-law model, and they are given below (Atlas et al. 1973; Chu et al. 1999; Su et al. 2004):

$$V = [9.65 - 10.3e^{-6D}] \tag{3}$$

$$V(D) = AD^B \tag{4}$$

Where A is in m $s^{-1}$ $cm^{-B}$; and B is dimensionless. In order to realize the discrepancy between these two models, we use measured data collected by a ground-based disdrometer to validate (3) and (4). The results are presented in Fig. 1, in which the solid line represents the power-law model and the dashed curve is the Atlas model and the scatter dots are the in-situ measured data taken on 21 May 2004. It is clear from Fig. 1 that in general both the power-law and Atlas models are in good agreement with observations. Detailed analysis shows that the power-law model fits better to the portion of larger raindrop size than to that of smaller drop size, and vice versa for the Atlas model. Note that the estimated values A and B for the power-law model obtained from the least squares fit are, respectively, A = 4.187 and B = 0.795, which are different from those reported by other researchers (Spilhaus 1948; Sekhon and Srivastava 1971; Atlas and Ulbrich 1977; Chu et al. 1999). A number of factors are responsible for the cause of the differences of the values of A and B obtained by different experiments, including the experimental instruments used to collect the raindrop size distribution data, rain type, deformation of the raindrop, the height that the experiment was carried out, level of 0°C isotherm, and so on (Chu et al. 1999). Therefore, the interpretation of the differences between experimental results should be cautious. It should be noted that (4) will be invalid when the diameter of a raindrop is more than 5.8 mm, because in this situation the raindrop will become unstable and will be split due to vibration and deformation of the raindrop itself (Gunn and Kinzer 1949).

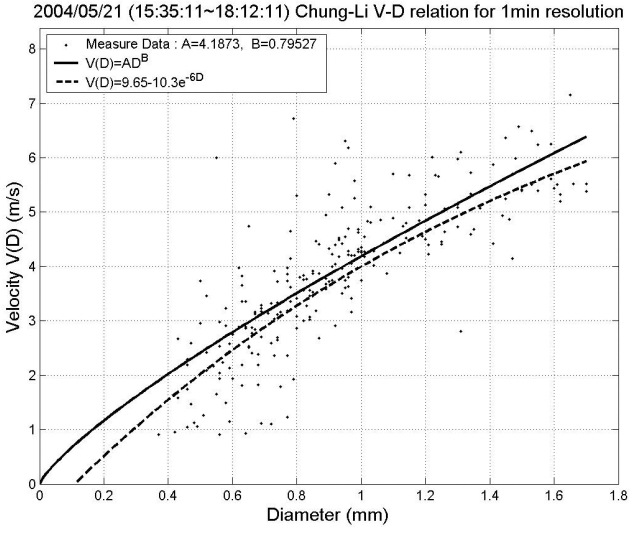


Fig. 1. Best fit of Power-Law (solid curve) and Atlas' empirical formulas (dashed curve) to observed data collected by disdrometer located on the campus of the National Central University.

Except for the relation between terminal velocity and raindrop diameter, the raindrop size distribution can also be obtained by using a disdrometer. The drop size distribution (DSD) N(D) induced from the measurements of the disdrometer is defined below:

$$N(D_i) = \frac{1}{\Delta t \cdot \Delta D} \cdot \sum_{j=1}^{M_i} \frac{1}{A_j \cdot v_j} \quad (m^{-3}\ mm^{-1}) \tag{5}$$

where i is the classification of drop size; $D_i$ is the mean diameter (mm) for the ith classification; $M_i$ is the total drop number during the sampling time $\Delta t$ (sec) for the ith classification; $\Delta D$ is the separation of the drop size classification (mm); $A_j$ is the effective measurement area of the disdrometer apparatus ($mm^2$) when observing the "j" drop; $v_j$ is the falling velocity of drops (m $s^{-1}$); and N(D) is the particle number per unit volume and unit radius increment ($m^{-3}$ $mm^{-1}$). Experimental results have shown that the drop size distribution can be well approximated to the Gamma function as defined below (Su et al. 2004):

$$N(D) = N_0 D^{\mu} \exp(-\delta D) \tag{6}$$

Where $N_0$ is in $m^{-3}$ $mm^{-1-\mu}$ ; $\delta$ is in $mm^{-1}$; and $\mu$ is dimensionless. From (6), we notice that the characteristics of the Gamma distribution are governed by three parameters of $N_0$, $\delta$, and $\mu$, which determine the mean, mode and variance of the distribution. Figure 2 presents an example of the disdrometer-observed raindrop size distribution collected on

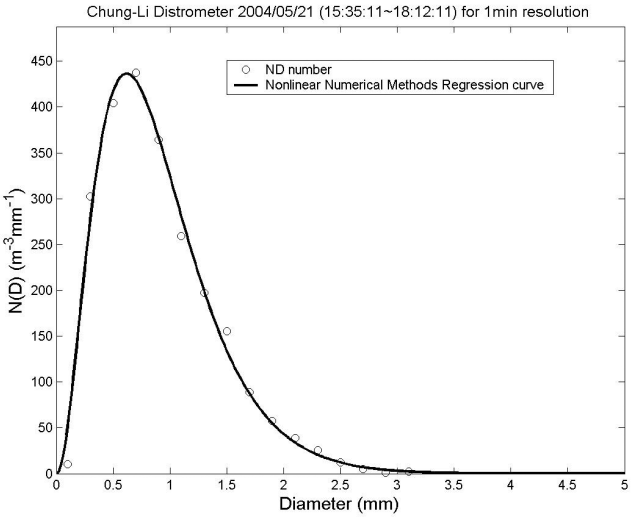


Fig. 2. Best fit curve of drop size distribution N(D) in Chungli region observed by using the numerical values method.

the campus of the National Central University, in which the solid curve is the best fit of (6) to the observed data points. It is obvious that the Gamma distribution function can perfectly describe the observed raindrop size distribution with the estimated values of $N_0 = 10961$, $\delta = 3.52$, and $\mu = 2.179$. In the following, with the relation between terminal velocity and diameter of the raindrop and the drop size distribution given above, the relation between specific attenuation of the EM wave at the Ka-band and the rain fall rate will be established in accordance with the Mie scattering theory.

To proceed, we introduce first volume scattering and extinction coefficients $\kappa_s$ and $\kappa_e$ which are, respectively, defined as the total scattering and total attenuation cross section areas in unit volume, and their units are $(N_p m^{-3}) \times m^2 = N_p m^{-1}$, which are the function of the drop size distribution and the scattering and attenuation cross sections. Note that $\kappa_s$ and $\kappa_e$ can also be, respectively, termed as scattering and total specific attenuations and expressed in unit of dB $km^{-1}$. Mathematically, $\kappa_s$ and $\kappa_e$ can be expressed in accordance with the following formula (Ulaby et al. 1981):

$$\kappa_e = \int_{r_1}^{r_2} p(r)\, Q_e(r)\, dr \tag{7}$$

$$\kappa_s = \int_{r_1}^{r_2} p(r)\, Q_s(r)\, dr \tag{8}$$

where $\kappa_s$ and $\kappa_e$ are, respectively, volume scattering and extinction coefficients ($N_p m^{-1}$); r is radius, which equals half diameter of D; p(r) is drop size distribution, i.e., the number of particle in unit volume and unit radius increment; $Q_s(r)$ is the scattering cross section area of the raindrop sphere with the radius of r ($m^2$); $r_1$ and $r_2$ represent the lower limit and upper limit of the raindrop radius (m). Commonly, in the volume of a cloud or rain area, the drop size distribution p(r) can be described as a continuous function, as one of the examples presented in (6). However, for some empirical drop size distributions, such as Laws-Parsons drop size distribution, only tabulated data are given. In this situation, p(r) can be obtained in accordance with the following approximate expression (Setzer 1970):

$$p(r) \approx \frac{R \cdot P_c(r)}{V(r) \cdot v_0(r)} \tag{9}$$

where r is diameter of a raindrop; R is the rain fall rate (mm $hr^{-1}$); $v_0(r)$ is the volume of a sphere with a radius of r ($m^3$); V(r) is the terminal velocity of drops; and $P_c(r)$ is the percentage of the drop size distribution (%). Once the drop size distribution N(r) is specified in the tabulated data sheet, $P_c(r)$ can be estimated in accordance with the following expression:

$$P_c(r) = \frac{N(r)}{\int N(r)\, dr} \times 100\% \tag{10}$$

For the purposes of numerical calculation, $\kappa_s$ and $\kappa_e$ can be expressed in terms of the scattering and extinction efficiency in the forms of $\xi_s = Q_s / \pi r^2$ and $\xi_e = Q_e / \pi r^2$ and the dimensionless parameter of $\chi = 2\pi r / \lambda_0$:

$$\kappa_s = \frac{\lambda_0^3}{8\pi^2} \int_0^\infty \chi^2\, p(\chi)\, \xi_s(\chi)\, d\chi \tag{11}$$

$$\kappa_e = \frac{\lambda_0^3}{8\pi^2} \int_0^\infty \chi^2\, p(\chi)\, \xi_e(\chi)\, d\chi \tag{12}$$

where the integral restriction is applied in the whole possible range of $\chi$ value, which implies that $p(\chi) = 0$ when $r < r_1$ and $r > r_2$. The volume attenuation coefficient $\kappa_e$ is the sum of the volume absorption coefficient $\kappa_a$ and volume scattering coefficient $\kappa_s$:

$$\kappa_e = \kappa_a + \kappa_s \tag{13}$$

where all the units of $\kappa_e$, $\kappa_s$, $\kappa_a$ are $N_p m^{-1}$. According to Mie theory, the expressions of the volume attenuation coefficient $\kappa_e$ and the volume absorption coefficient $\kappa_a$ can be formulated below (Ulaby et al. 1981):

$$\xi_s(n, \chi) = \frac{2}{\chi^2} \sum_{l=1}^{\infty} (2l+1)\left( |a_l|^2 + |b_l|^2 \right) \tag{14}$$

$$\xi_e(n, \chi) = \frac{2}{\chi^2}\sum_{l=1}^{\infty}(2l+1)\,\mathrm{Re}\{a_l + b_l\} \tag{15}$$

where Re represents the real parts of Mie coefficients $a_l$ and $b_l$ that are the function of n and $\chi$. In order to facilitate numerical computation using a computer, on the basis of recursive relations of the Bessel function, Deirmendjian (1969) developed an algorithm to calculate the Mie coefficients $a_l$ and $b_l$ as follows:

$$a_l = \frac{\left(\frac{A_l}{n} + \frac{1}{\chi}\right)\mathrm{Re}\{W_l\} - \mathrm{Re}\{W_{l-1}\}}{\left(\frac{A_l}{n} + \frac{1}{\chi}\right)W_l - W_{l-1}} \tag{16}$$

$$b_l = \frac{\left(nA_l + \frac{1}{\chi}\right)\mathrm{Re}\{W_l\} - \mathrm{Re}\{W_{l-1}\}}{\left(nA_l + \frac{1}{\chi}\right)W_l - W_{l-1}} \tag{17}$$

where

$$W_l = \left(\frac{2l-1}{\chi}\right)W_{l-1} - W_{l-2} \tag{18}$$

$$A_l = -\frac{1}{n\chi} + \left[\frac{1}{n\chi} - A_{l-1}\right]^{-1} \tag{19}$$

$$W_0 = \sin\chi + j\cos\chi \tag{20}$$

$$W_{-1} = \cos\chi - j\sin\chi \tag{21}$$

$$A_0 = \cot n\chi \tag{22}$$

Where n is the complex refractive index of the raindrop and expressed as:

$$n = n' - jn'' \tag{23}$$

Where n' is the real part and n" is the imaginary part of the index of refraction. Figure 3 shows the variations of the Mie scattering efficiency $\xi_e$ and attenuation efficiency $\xi_s$ with $\chi$. As indicated, the magnitudes of $\xi_e$ and $\xi_s$ will be saturated when $\chi$ is greater than 1. It implies from (1) that the saturation of the attenuation of the EM wave amplitude will occur when the radius of the raindrop is greater than $\lambda_b$, which is the wavelength of the electromagnetic waves in the background medium.


Fig. 3. Calculated Mie coefficients at 19.5 GHz.

Once the Mie scattering efficiency $\xi_e$ and attenuation efficiency $\xi_s$ are obtained and the raindrop distribution N(r) is given, we can compute the corresponding specific attenuations (i.e., $\kappa_s$ and $\kappa_e$) in terms of (11) and (12). Note that the rain fall rate, R, is related to N(r) in accordance with the following expression:

$$R = \frac{\pi}{6}\int N(r)\, r^3\, V(r)\, dr \quad \text{(in continuous form)} \tag{24a}$$

$$= 6\pi \times 10^{-4}\sum_{i=1}^{N} V_i r_i^3 \quad \text{(in discrete form)} \tag{24b}$$

where in (24b) the unit of R is mm $hr^{-1}$; $V_i$ is terminal velocity (m $s^{-1}$); $r_i$ is the diameter of the ith raindrop (mm); and N is the total number of the rain drops per unit volume. Note from (24a) and (11) and (12) that the specific attenuations $\kappa_s$ and $\kappa_e$ should be the functions of the rain fall rate. Therefore, the analytical relations between the specific attenuations and the rain fall rate can be derived, provided the mathematical expressions of N(r) and V(r) are both given. In fact, the analytical relation between $\kappa_e$ and R for Laws-Parsons and Marshall-Palmer raindrop distributions have been established by Olsen et al. (1978), which is shown to be of the form of $\kappa_e = aR^b$. The magnitudes of a and b for Laws-Parsons and Marshall-Palmer distributions at 19.5 GHz are that: $a_{LP} = 0.0631$, $b_{LP} = 1.111$, $a_{MP} = 0.0529$, and $b_{MP} = 1.1299$.

## 3. EXPERIMENTAL SYSTEMS

### 3.1 Ka-Band Dual Circular Polarization Reflector Antenna System

The 19.5 GHz Dual Circular Polarized Radar System,

which was established in 2003 for the purposes of studying rain and atmospheric attenuations of electromagnetic wave propagation with in the Ka-band over the Taiwan area, was implemented on the campus of the National Central University, Chungli City, Taiwan, with both its transmitting and receiving dish antennas located on the top of VHF radar buildings and without any obstacles obstructing the transmission path of signals. Because the distance between transmitting and receiving antennas must be in the far field, the distance between transmitting and receiving antennas is approximately 158 meters, which is greater than the minimum far field distance of 115 meters specified for the radar system. The antenna at the transmitting end is the same as that at the receiving end, i.e., the antennas are Cassergain Disc Antennas of diameter of 0.94 m. In addition to the radar system, we set up a 2D disdrometer, an automatic weather station and an optical rain gauge in the radar field to carry out precipitation measurements for the study of rain and atmospheric attenuations of 19.5 GHz electromagnetic wave propagation in the troposphere. Table 1 shows detailed electrical specifications of both the transmitting and receiving ends of the Ka-band radar system. Our experimental system is shown in Fig. 4.

### 3.2 Optical Rain Gauge

The rain gauge collecting the surface precipitation data is an essential tool in performing rain attenuation experiments (Crane 1980; Crane 2003). The rain gauges employed for the propagation experiment are ScTI's (Scientific Technology, Inc.) Series optical rain gauges (ORG), which

Table 1. Specifications for Ka-band Dual Circular Polarization Reflector Antennas System.

| **Transmitter Box** | **Spec.** |
|---|---|
| Output Power | 10 ± 0.4 dBm |
| Output Power Stability | ≦ 0.2 dB |
| Input Power Range | -40 to -10 dBm |
| Input VSWR | ≦ 1.2 |
| Feed Isolation | ≧ 40dB |
| **Receiver Box** | |
| LNA Gain | 30 dB ± 2.5 dB |
| IF Amplifier Gain | 10 ± 1 dB |
| Total Amplifier Gain Stability | ≦ 0.2 dB |
| IF Output Frequency | 1 ~ 16 GHz (2GHz) |
| IF Output Frequency Stability | ≦ 200 ppm |
| IF Output Spurious | ≦ 50 dBc |
| IF VSWR | ≦ 1.2 |
| Feed Isolation | ≧ 40 dB |
| RF Switch Setting Time | ≦ 0.01ms |
| Input Power Range | -25 to -55 dBm |

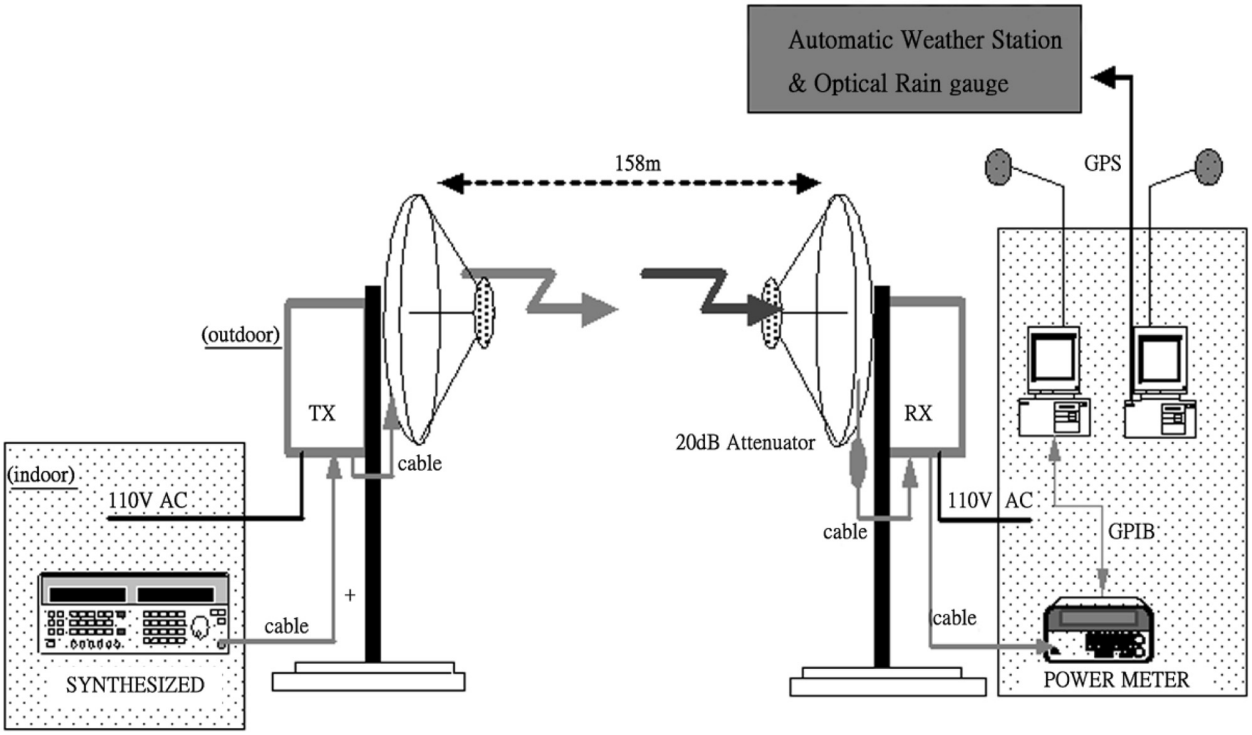


Fig. 4. Schematic diagram of the experimental system at the National Central University.

can provide accurate measurement of precipitation in all weather conditions with high temporal resolution. This kind of rain gauge, designed for rugged, unattended operation, has been proven in adverse environments, including land sites, ocean deployed data buoys and shipboard. The sensors offer easy field calibration capability and a simplified interface for data loggers and data acquisition systems. Precipitation is measured by detecting the optical irregularities induced by drops falling through an infrared optical beam. These irregularities causing the scintillation of signals have characteristic patterns which are detected by the sensor and converted to precipitation. ScTI Optical Rain Gauges are not affected by many of the environmental factors which cause significant errors with traditional rain gauges. Detailed characteristics of optical rain gauge Model ORG-815 are summarized in Table 2.

### 3.3 Disdrometer

The drop-size distribution of the hydrometeor in the path of the Earth-satellite communication link is a vitally important parameter in the investigation of rain attenuation. Although the measurement of drop-size distribution aloft by using a VHF radar has been reported (Wakasugi et al. 1986), drop-size distribution near the ground cannot be obtained by VHF radar. The only one way to measure surface drop-size distribution is to use a ground-based disdrometer. Besides distribution of the hydrometeor, many precipitation-related parameters, such as rain fall rate and the shape of the hydrometeor, can also be obtained through disdrometer measurements. The disdrometer employed for the propagation experiment reported in this article is the 2D-Video-Distrometer. For each raindrop, snowflake, or hailstone reaching the measuring area, the front view, side view and velocity can be measured and recorded using this instrument. The resolution of the digitizing grid is of the order of 0.25 mm; and a reliable classification of precipitation event distributions for size and velocity of particles as well as of oblateness of drops can be generated in real time using this equipment. A detailed description of the characteristics of the 2D-Video-Disdrometer is summarized in Table 3.

Table 2. Characteristics of Optical Rain Gauge (Model ORG-815).

| ORG | Characteristics |
|---|---|
| Measure Range | 0.1 ~ 500 mm $hr^{-1}$ |
| Accuracy | 5% |
| Resolution | 0.001 mm |
| Rain Accumulation | 0.001 ~ 999.9 mm |
| Time Constant | 10 seconds |
| Data Update Rate | Every 5 seconds |
| Supply Voltage | 11 - 16 VDC |
| Current Drain | 500 - 800 mAmp |
| Signal Output | RS-232 |
| Operational Environment | |
| - Temperature | 40 to 50°C |
| - Relative Humidity | 0 - 100% |
| Size | 30”L × 18”W × 12”H |
| Weight | 25 lb |
| Cable Length | 15 meters |

### 3.4 Automatic Weather Station

The main objective of the automatic weather station is to provide real time weather data for simultaneous analysis of prevailing weather conditions when performing the transmission channel experiment in the Ka-band. The apparatus in this station include: a wind velocity anemoscope, thermometer, humidity meter, air barometer, and a rain gauge etc. The observed meteorological data are recorded automatically and stored in the computer. This allows for real time recordings of, wind velocity, wind direction, temperature, relative humidity and atmospheric pressure etc. The minimum time resolution of the recorded weather data is 30 sec/sample, and the observation resolution of this experiment is 1 min/sample.

## 4. OBSERVATIONAL RESULTS AND DISCUSSIONS

Employing an approximation based on the absorption lineshape profiles of Van Vleck and Weisskopf (Ippolito 1986), the value of specific attenuation at a frequency of

Table 3. Characteristics of 2D-Video-Disdrometer.

| Disdrometer | Characteristics |
|---|---|
| Measure Range | 100 × 100 $mm^2$ |
| Vertical Velocity Accuracy | > 5 % |
| Resolution (horizontal) | > 0.22 mm |
| Resolution (vertical) | > 0.3 mm , < 10 m $s^{-1}$ |
| Integration Time | 15 sec ~12 hours |
| Supply Voltage | 110/220/240/V, 50/60 Hz |
| Power Consumption | 500 W |
| Operating Temperature | -10 to 40°C |
| Survival Temperature | -20 to 60°C |
| Weight | 130 Kg |
| Height | 110 cm |
| Width | 60 cm |
| Length | 150 cm |

19.5 GHz can be estimated for a density of water vapor concentration of 28 g $m^{-3}$; it is about 0.3 dB $km^{-1}$. Consequently, whilst water vapor conditions were quite dense at the location of the experiment, total attenuation produced by the dense water vapor was only about 0.0474 dB. This occurred over a distance of 158 meters, i.e., that distance between the transmitting and receiving antennas in the radar system. Compared with rain attenuation, the contribution to 19.5 GHz electromagnetic wave attenuation by water vapor absorption in our experimental field is very small and can be ignored.

As mentioned in the above section, from Mie theory, we know that the relation between the rain fall rate and specific attenuation can be expressed as $\kappa_e = aR^b$ (Olsen et al. 1978), where $\kappa_e$ is the specific attenuation coefficient (dB $km^{-1}$), i.e., attenuation value per unit length; R is the point rain fall rate on the surface; and a and b are the coefficients relating to the frequency of radio waves, drop size distribution, and rain temperature. Figure 5 shows a rain attenuation event observed by a 19.5 GHz bistatic radar system on 24 August 2004. The received power (upper panel), measured specific attenuation (middle panel) and the surface rain fall rate (bottom panel) are displayed. It is clear from Fig. 5 that there is a one-to-one correspondence between the rain fall event and remarked enhancement (severe attenuation) of specific attenuation (received power). A maximum specific attenuation of 10 dB $km^{-1}$ (corresponding to a maximum rain fall rate of 90.6 mm $hr^{-1}$) was recorded. Once the specific attenuation $\kappa_e$ and rain fall rate R are measured simultaneously, a power-law relation between specific attenuation and the rain fall rate of the form: $\kappa_e = aR^b$ can be employed to best fit to the measured data such that the values of the coefficient a and the power b can be estimated. As a result, the precipitation effect on Ka-band EM wave propagation can be quantitatively estimated and the rain attenuation model for a specific terrestrial propagation link is thus established.

A number of empirical drop size distributions, including Laws-Parsons, Marshall-Palmer, Wexler and Best, are extensively used in modeling observed drop size distribution for estimating rain attenuations. Of these, Laws-Parsons and Marshall-Palmer models are used most frequently (Ulaby et al. 1981). An important issue is the discrepancy between results of in-situ measurements and empirical models. Figure 6 presents a scatter diagram of observed specific attenuation versus the rain fall rate. The diagram was scaled from Fig. 5 at 10-s time resolution, in which dots represent observed data points and the solid curve is the line of best fit based on the power-law relation $\kappa_e = aR^b$. The other two curves are realizations of the models of Laws-Parsons and Marshall-Palmer drop size distributions (Ulaby et al. 1981). From the results presented in Fig. 6, we find that in general our experimental results of rain attenuation in the Ka-band are slightly larger than the results predicted by the models of empirical rain drop size distributions. This discrepancy varies positively with the rain fall rate.

In order to assess the overall performance of the empirical models employed for the estimation of rain attenuations at 19.5 GHz, we analyze the data collected by the terrestrial propagation link located on the campus of the National Central University during 2004 to obtain specific attenuation. The total duration of the measured rain attenu-

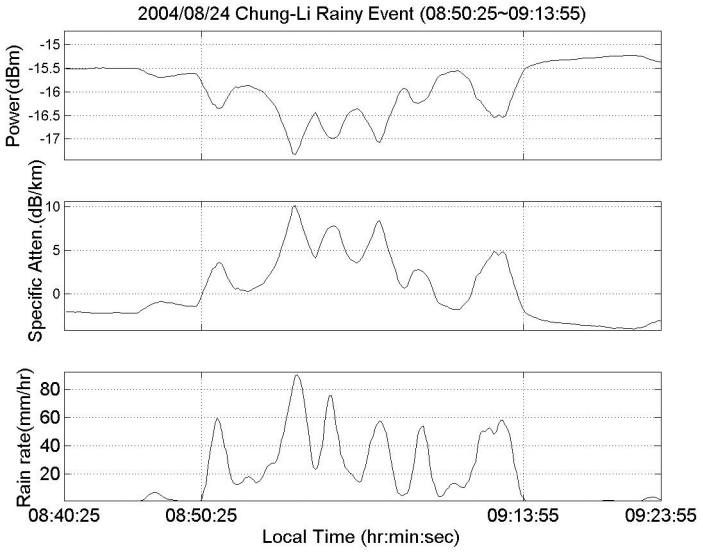


Fig. 5. Observation data on 24 August 2004. The receiving power, conversion specific attenuation, and rain rate are displayed respectively in time sequence from top to bottom.

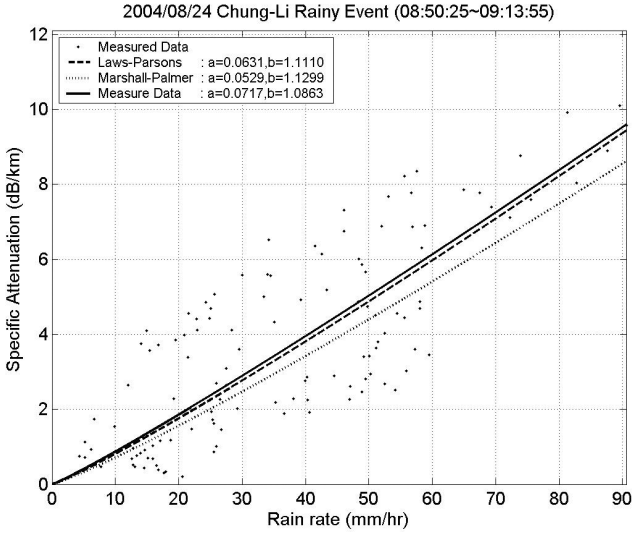


Fig. 6. Relation of rain rate and specific attenuation for the data scaled from Fig. 5. The dots represent the observed data points, while the solid line is the line of best fit based on the relation of specific attenuation and rain rate in $\kappa_e = aR^b$. The other two dash lines are the estimated theoretical values of rain attenuation based on Laws-Parsons and Marshall-Palmer drop size distributions.

ation events occurring in 2004 was about 21 hr and 25 min. Figure 7 shows the statistical result, in which the line of best fit made from disdrometer-measured (solid) raindrop distribution, and the curves calculated from Laws-Parsons (dashed) and Marshall-Palmer (dot-dashed) drop size distributions are shown. From the figure, we can note that empirical rain drop distribution models will underestimate rain attenuations at 19.5 GHz, especially in the case of a high rain fall rate. The estimated coefficient a and power b in the best fitted power-law relation $\kappa_e = aR^b$ deduced from long-term measurement are, respectively, a = 0.0699 and b = 1.0984. Quantitative estimation indicates that the differences between the specific attenuations calculated from the best fit relation and the empirical relations are, respectively, about 0.3 dB km$^{-1}$ for L-P drop size distribution and 0.7 dB km$^{-1}$ for M-P drop size distribution at R = 50 mm hr$^{-1}$. Therefore, a considerably large error in the estimation of the rain attenuation will be induced if the propagation path length is long enough. From this result we conclude that the empirical rain drop size distribution used for the estimation of the rain attenuation in the Ka-band over Taiwan region may not be a best choice and the use of a correct expression that is obtained through long-term statistics and careful analysis is strongly suggested.

From the discussions made in section 2, it is obvious from (11) and (12) that different raindrop size distributions and terminal velocity-drop size relations will give rise to different $\kappa_s$-R and $\kappa_e$-R relations. Figure 8 presents examples of $\kappa_s$-R and $\kappa_e$-R relations for the disdrometer-observed raindrop size distribution taken on 21 May 2004, on the campus of the National Central University, in which the power-law model of the terminal velocity-rain drop size relation as shown in (4) is employed for computation. As shown, variation of specific attenuation with the rain fall rate can be well approximated to a straight line in a log-log chart, strongly indicating a power-law relation between them. Moreover, the magnitude of the specific attenuation due to EM wave scattering is much smaller than that due to the absorption effect of water content in a raindrop by one order of magnitude or more. As a matter of fact, the total rain attenuation in the Ka-band is almost completely attributable to absorption by raindrops, and scatter loss only plays a very minor role. Figure 9 shows another example of $\kappa_s$-R and $\kappa_e$-R relations, in which the data are the same as is Fig. 8 and the V-r empirical relation as shown in (3) is used for computation. The results shown in Fig. 9 are very similar to those presented in Fig. 7, except for the former being slightly larger than the latter by a factor of less than 20%.

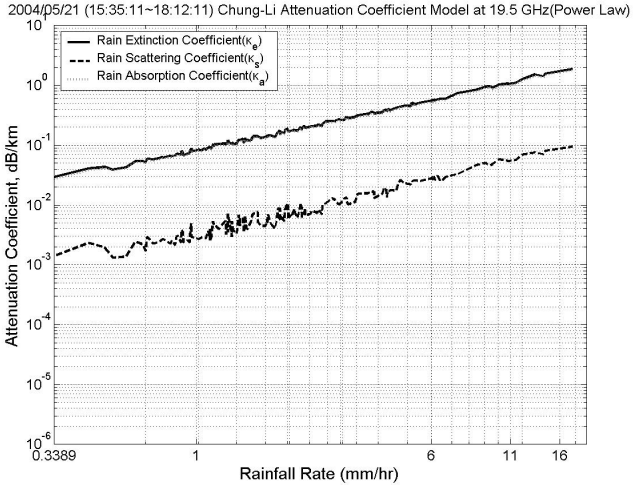


Fig. 8. Results of specific attenuation at the frequency of 19.5 GHz based on the hypothesis of Power-Law by using an example of observation data on 21 May 2004.

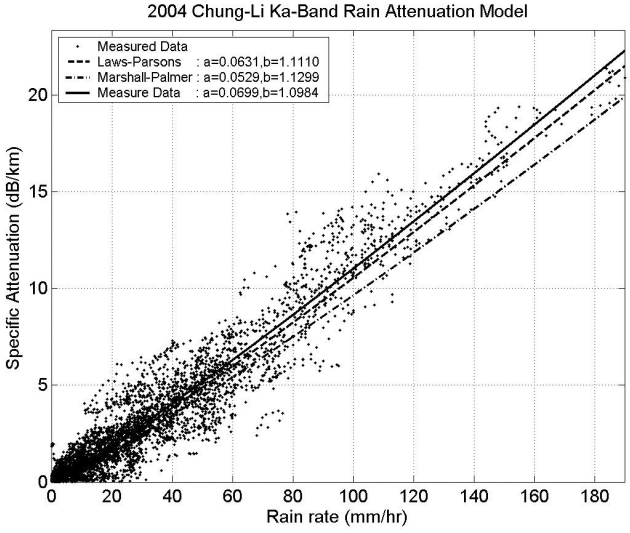


Fig. 7. Relation of surface rain rate and specific attenuation in all the observation data of 2004. The maximum rain rate is 190 mm hr$^{-1}$.

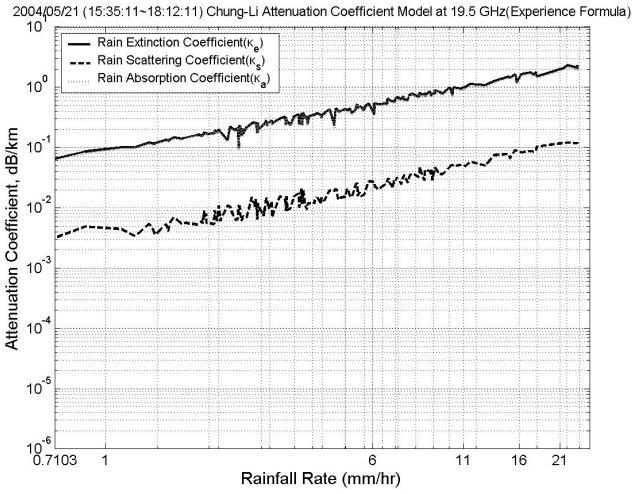


Fig. 9. Results of specific attenuation at the frequency of 19.5 GHz based on the hypothesis of Atlas empirical formula (3) by using an example of observation data on 21 May 2004.

## 5. CONCLUSIONS

On the basis of disdrometer-measured raindrop size distribution data and rain attenuation of 19.5 GHz EM waves collected by a terrestrial propagation system located on the campus of the National Central University, we theoretically and experimentally analyze the relation between specific attenuation and the rain fall rate in the Ka-band. We find that water absorption of EM waves propagating through raindrops is the major cause of rain attenuation at 19.5 GHz, and that scattering of EM waves interacting with discrete raindrops on observed rain attenuation is very minor and can be ignored. Regression analysis shows that the relation between specific attenuation $\kappa_e$ and the rain fall rate, R, follows the power law $\kappa_e = aR^b$, where the coefficient a and the power b are, respectively, estimated to be 0.0699 and 1.0984. These are different to those estimated by the empirical Laws-Parsons and Marshall-Palmer drop size distributions. The discrepancies in a and b values between experimental results and empirical expressions leads to a difference of 0.3 - 0.7 dB $km^{-1}$ in the estimation of specific attenuations for a rain fall rate of 50 mm $hr^{-1}$. Therefore, the use of a correct $\kappa_e$-R relation to obtain more accurate estimation of rain attenuation is highly recommended.

**Acknowledgements** This work was supported by National Space Program Office (NSPO) of The Republic of China under grants NSC90-NSPO(A)-ECP-008-01, NSC91-NSPO (A)-ECP-008-01, and 92-NSPO(B)-ECP-008-01. S. P. Shih would like to thank Dr. C. L. Su, Mr. A. H. Chou and other friends for their helps in implementing the terrestrial propagation system and analyzing rain and radar data.

## REFERENCES

Atlas, D. and C. W. Ulbrich, 1977: Path- and area-integrated precipitation measurements by microwave attenuation in the 1-3 cm band. *J. Appl. Meteorol.*, **16**, 1322-1331.

Atlas, D., R. C. Srivastava, and R. S. Sekon, 1973: Doppler radar characteristics of precipitation at vertical incidence. *Rev. Geophys. Space Phys.*, **11**, 1-35.

Battan, L. J., 1973: Radar observation of the atmosphere. The University of Chicago Press, Ltd., London, 324 pp.

Bussey, H. E., 1950: Microwave attenuation statistics estimated form rainfall and water vapor statistics. *Proc. IRE*, **38**, 781-785.

Chu, Y. H., S. P. Shih, C. L. Su, K. L. Lee, T. H. Lin, and W. C. Liang, 1999: A study on the relation between terminal velocity and VHF backscatter from precipitation particles using the Chung-Li VHF Radar. *J. Appl. Meteorol.*, **38**, 1720-1728.

Crane, R. K., 1971: Propagation phenomena affecting satellite communication systems operating in the centimeter and millimeter wavelength bands. *Proc. IEEE*, **59**, 173-188.

Crane, R. K., 1980: Prediction of attenuation by rain. *IEEE Trans. Commun.*, **COM-28**, 1717-1733.

Crane, R. K., 1996: Electromagnetic wave propagation through rain. New York, Wiley, 273 pp.

Crane, R. K., 2003: A local model for the prediction of rain-rate statistics for rain-attenuation models. *IEEE Trans. Antennas Propag.*, **51**, 2260-2273.

Deirmendjian, D., 1969: Electromagnetic scattering on spherical polydispersions. American Elsevier Publishing Co., Inc., New York.

Dissanayake, A., J. Allnutt, and F. Haidara, 1997: A prediction model that combines rain attenuation and other propagation impairments along earth-satellite paths. *IEEE Trans. Antennas Propag.*, **45**, 1546-1558.

Gunn, R. and G. D. Kinzer, 1949: The terminal velocity of fall for water droplets instagent air. *J. Meteorol.*, **6**, 243-248.

Harrold, T. W., 1967: Attenuation of 8.6 mm wavelength radiation in rain. *Proc. Inst. Elec. Eng.*, **114**, 201 pp.

Hasanuddin, Z. B., K. Fujisaki, K. Ishida, and M. Tateiba, 2002: Measurement of ku-band rain attenuation using several VSATs in Kyushu island, japan. *IEEE Antennas Wireless Propag. Lett.*, **1**, 116-119.

Hogg, D. C. and T. H. Chu, 1975: The role of rain in satellite communication. *Proc. IEEE*, **63**, 1308-1331.

Ippolito Jr., L. J., 1986: Radiowave propagation in satellite communication. Van Nostrand Reinhold Company, New York, 241 pp.

Karasawa, Y. and Y. Maekawa, 1997: Ka-band earth-space propagation research in Japan. *Proc. IEEE*, **85**, 821-842.

Oguchi, T., 1983: Electromagnetic wave propagation and scattering in rain and other hydrometeors. *Proc. IEEE*, **71**, 1029-1078.

Olsen, R. L., D. V. Rogers, and D. B. Hodge, 1978: The aRb relation in the calculation of rain attenuation. *IEEE Trans. Antennas Propag.*, **AP-26**, 318-329.

Polonio, R. and C. Riva, 1998: ITALSAT propagation experiment at 18.7, 39.6 and 49.5 GHz at Spino D'Adda: three years of CPA statistics. *IEEE Trans. Antennas Propag.*, **46**, 631-635.

Rice, P. L. and N. R. Holmberg, 1971: Cumulative time statistics of surface-point rainfall rates. *IEEE Trans. Commun.*, **COM-21**, 1131-1136.

Samplak, R. A. and R. H. Turrin, 1969: Some Measurements of Attenuation by Rainfall at 18.5 GHz. *Bell Syst. Tech. J.*, **48**, 1767.

Sekhon, R. S. and R. C. Strivastava, 1971: Doppler radar observations of drop-size distributions in a thunderstorm. *J. Atmos. Sci.*, **28**, 983-994.

Setzer, D. E., 1970: Computed Transmission through rain at microwave and visible frequencies. *Bell Syst. Tech. J.*, **49**, 1873-1892.

Shih, S. P. and Y. H. Chu, 1999: Ka band propagation ex-

periments of experimental communication payload (ECP) on ROCSAT-1 - Preliminary Results. *Terr. Atmos. Ocean. Sci.*, **Suppl. Issue**, 145-146.

Spilhaus, A. F., 1948: Raindrop size, shape, and falling speed. *J. Meteorol.*, **5**, 108-110.

Su, C. L., Y. H. Chu, and C. Y. Chen, 2004: Analyzing the relationship between terminal velocity of raindrops and VHF backscatter from precipitation. *Terr. Atmos. Ocean. Sci.*, **15**, 629-646.

Ulaby, F. T., R. K. Moore, and A. K. Fung, 1981: Microwave remote sensing: Active and Passive. Vol. I, Addison-Wesley Publishing Company, Inc.

Wakasugi, K., A. Mizutani, M. Masaru, S. Fukao, and S. Kato, 1986: A direct method for deriving drop-size distribution and vertical air velocities from VHF doppler radar spectra. *J. Atmos. Ocean. Technol.*, **3**, 623-629.